Supplemental material for 'Eliminating object prior-bias from sparse-projection tomographic reconstructions'

July 25, 2020

Contents

1 An alternate method to compute weights-map

The value of k (discussed in Sec.10(C) of the main paper) is typically dependent on the number of false positives the system can allow in exchange for the detection of more true positives (regions of new changes). It is this choice and not the particular type of dataset that affects the selection of k. In our work, the chosen k corresponds to the one that gives minimal tolerance to false positives.

However, in case one wishes to completely avoid the use of this hyperparameter, one can construct a binary weights-map using an alternate method described below.

1. For the purposes of training, treat one of the previously scanned images as test.

2. Annotate the region of differences between the test and all of the previously scanned images based on domain knowledge.

3. Compute the difference between the pilot reconstruction of the test and its projection onto the eigenspace. Let this spatial map be called 'error map'.

4. Train a Support Vector Machine (SVM) model to classify patches of this error-map image into one of the two categories: new changes present, new changes absent.

5. Once the trained SVM model is obtained, it can be applied to generate binary weights-map for new test images in the same longitudinal study.

6. Once the binary weights-map $\boldsymbol{W_b}$ is obtained, the prior and the pilot can be stitched by $\boldsymbol{R} = \boldsymbol{W_b}(\text{Pilot}) + (1 - \boldsymbol{W_b})(\text{Prior})$. Fig. 1 shows results of this method on 2D okra dataset.

   Alternatively, these binary weights can also be used in the optimization loop in Eq. 1 (corresponding to Eq. 6 in the main paper), although this approach has not been pursued here.

$$J_3(\boldsymbol{\theta}, \boldsymbol{\alpha}) = \|\boldsymbol{\mathcal{R}x} - \boldsymbol{y}\|_2^2 + \lambda_1 \|\boldsymbol{\theta}\|_1 + \lambda_2 \|\boldsymbol{W_b}(\boldsymbol{x} - (\boldsymbol{\mu} + \sum_k \boldsymbol{V_k}\alpha_k))\|_2^2. \quad (1)$$

(a)   (b)   (c)

(d)   (e)   (f)
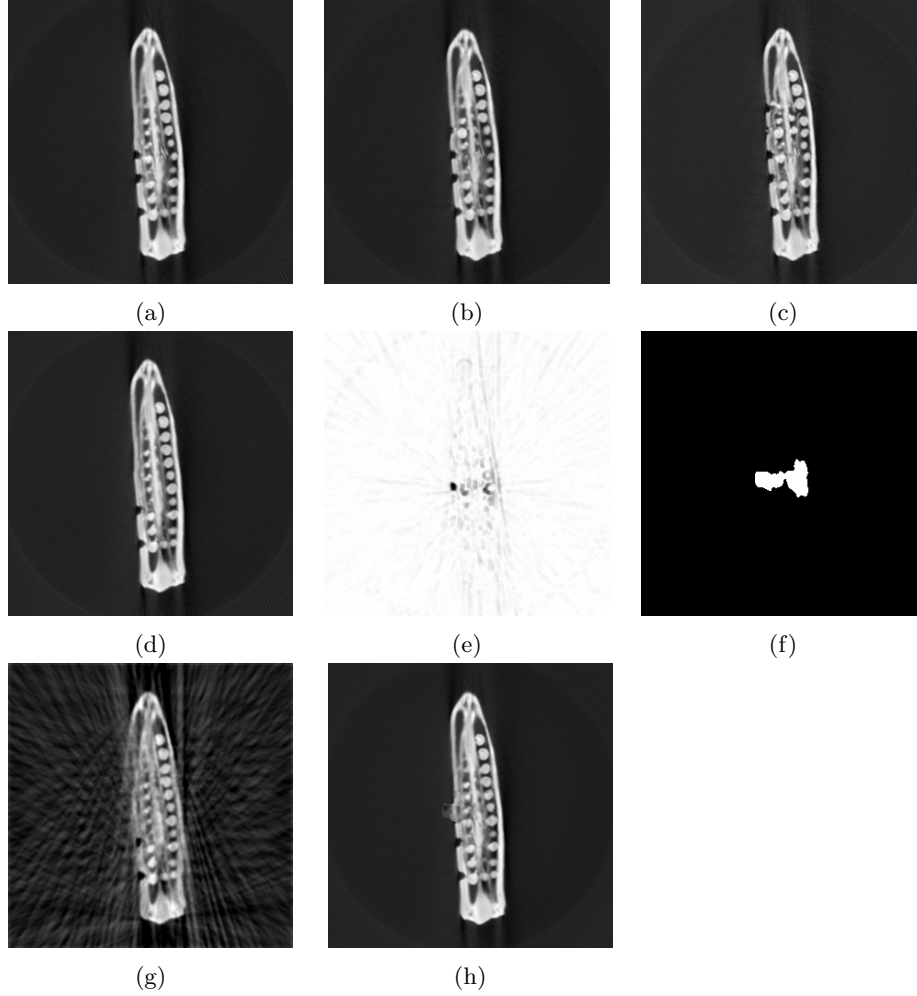
(g)   (h)

Figure 1: Using an alternate approach to generate (binary) weights map. (a)-(c) the images used as object-prior, (d) the test (310×310). Measurements along 60 views were taken. (e) error-map showing new regions, (f) detected binary weights map showing regions of new changes, (g) pilot, (h) final reconstruction with pilot in the new regions, and prior in the other regions.

2 Links to view our 3D reconstructions

The 3D reconstructions, corresponding to the images shown in Figs. 14, 16 and 19 in the main paper, can be better visualized in the form of a video. Hence, please refer to the following videos to view the 3D datasets and reconstruction results:

- **Okra:**

  https://www.dropbox.com/sh/x3yjfzsc5633d1t/AAAaVOXvTbc06a2DomPO1kSna?dl=0

- **Potato:**

  https://www.dropbox.com/sh/6mja5uh8fa2h0fc/AAA2h4VsLxAiXcEIhmTlM1xha?dl=0

- **Sprouts:**

  https://www.dropbox.com/sh/qtgeyckvbxiaz3s/AADhR2zRUUN4qXSXraErcqSea?dl=0

3 Larger images for reconstruction results

All the images shown in the main paper are displayed in small size due to space constraints. This restricts visualization of the structural details within them. Therefore, we present each of those images in large size here in order to view their internal structures with better clarity.
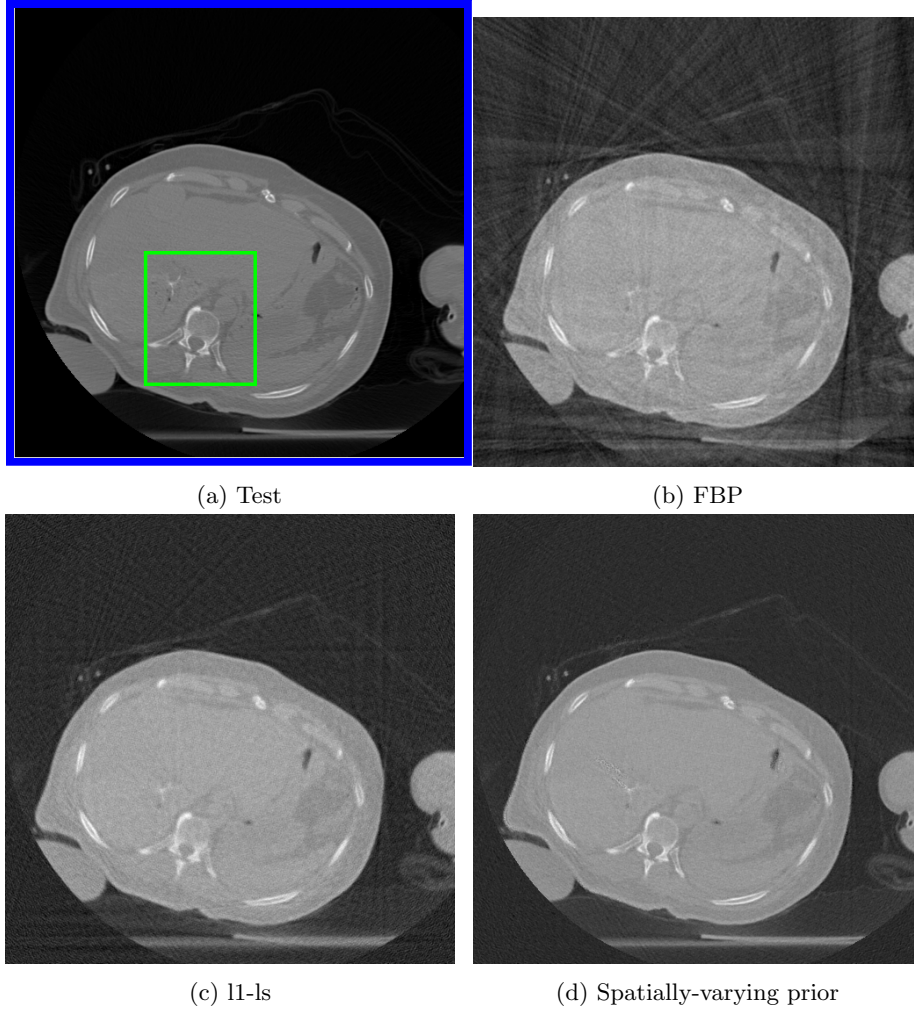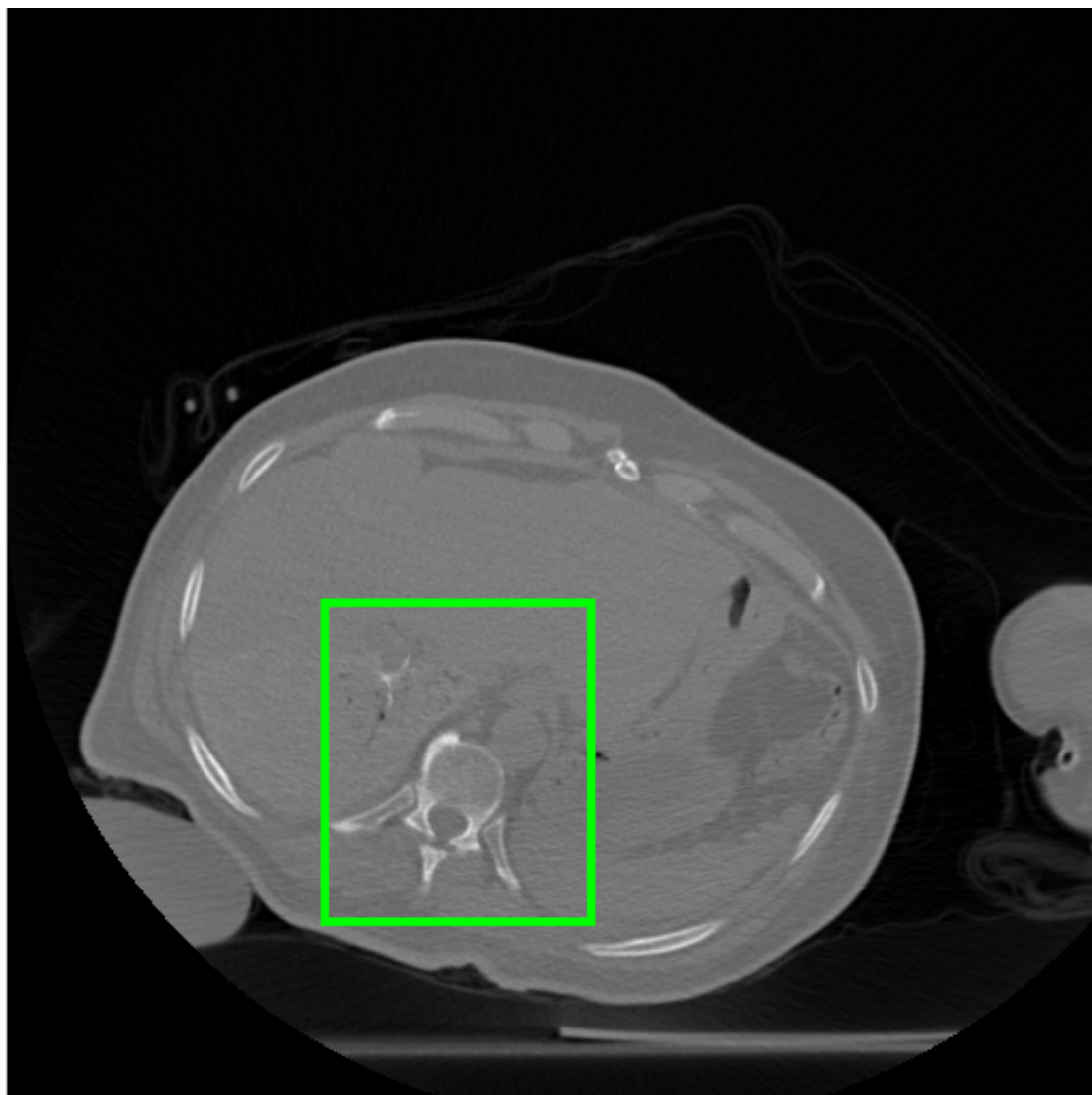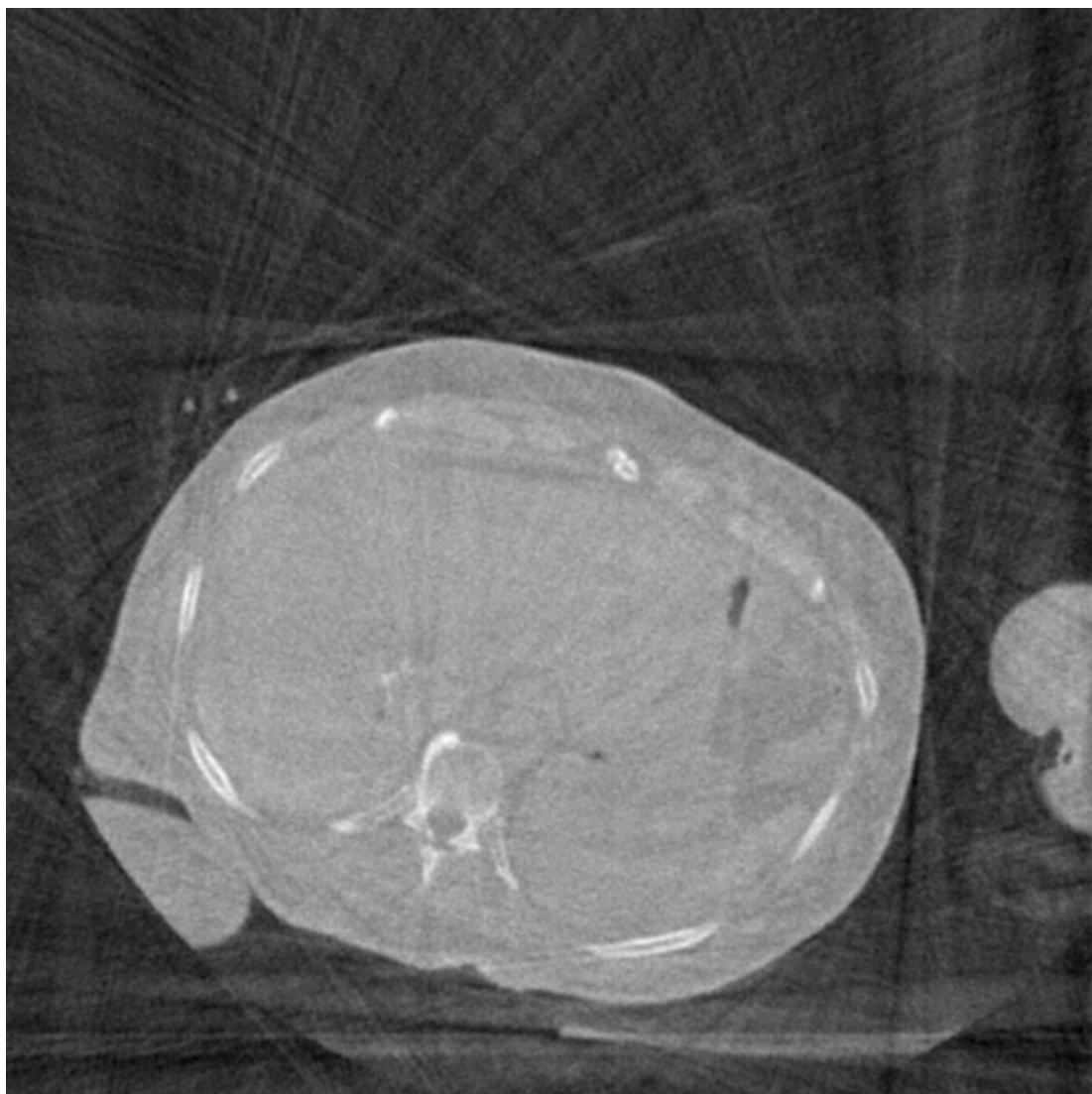
3.1 Liver

(a) Test

(b) FBP

(c) l1-ls

(d) Spatially-varying prior

Figure 2: Reconstruction of Liver corresponding to Figure 8 of the main paper.

Test image in Figure **2** is shown in large size for better clarity.

Test slice

Reconstruction result of Figure 2 is shown in large size for better clarity.
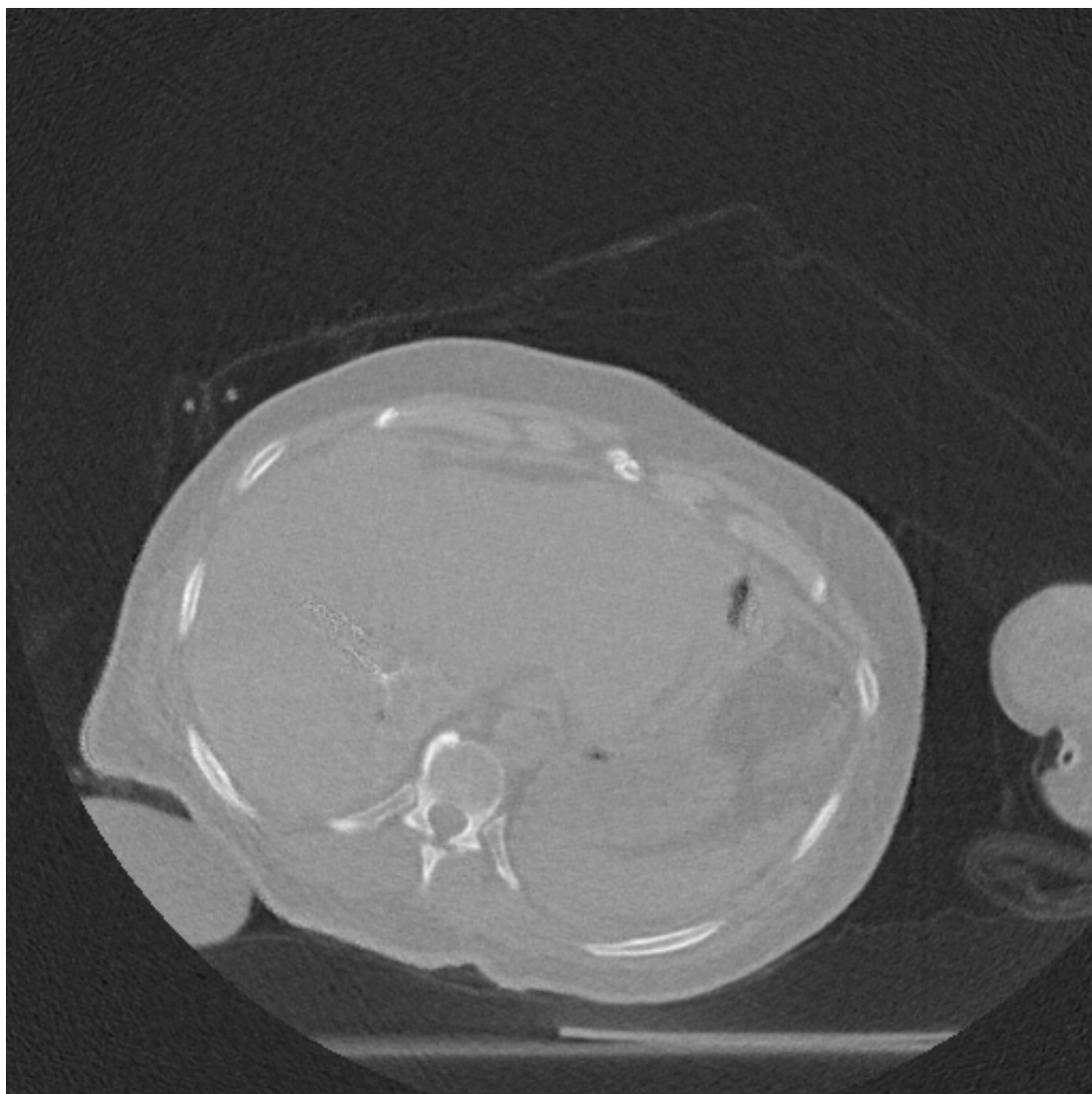

FBP

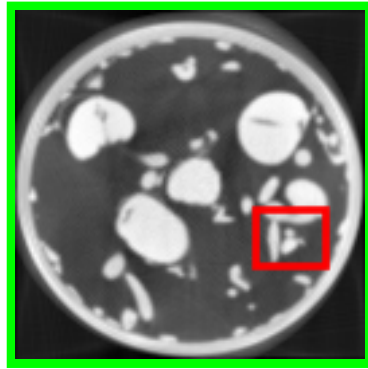Reconstruction result of Figure 2 is shown in large size for better clarity.
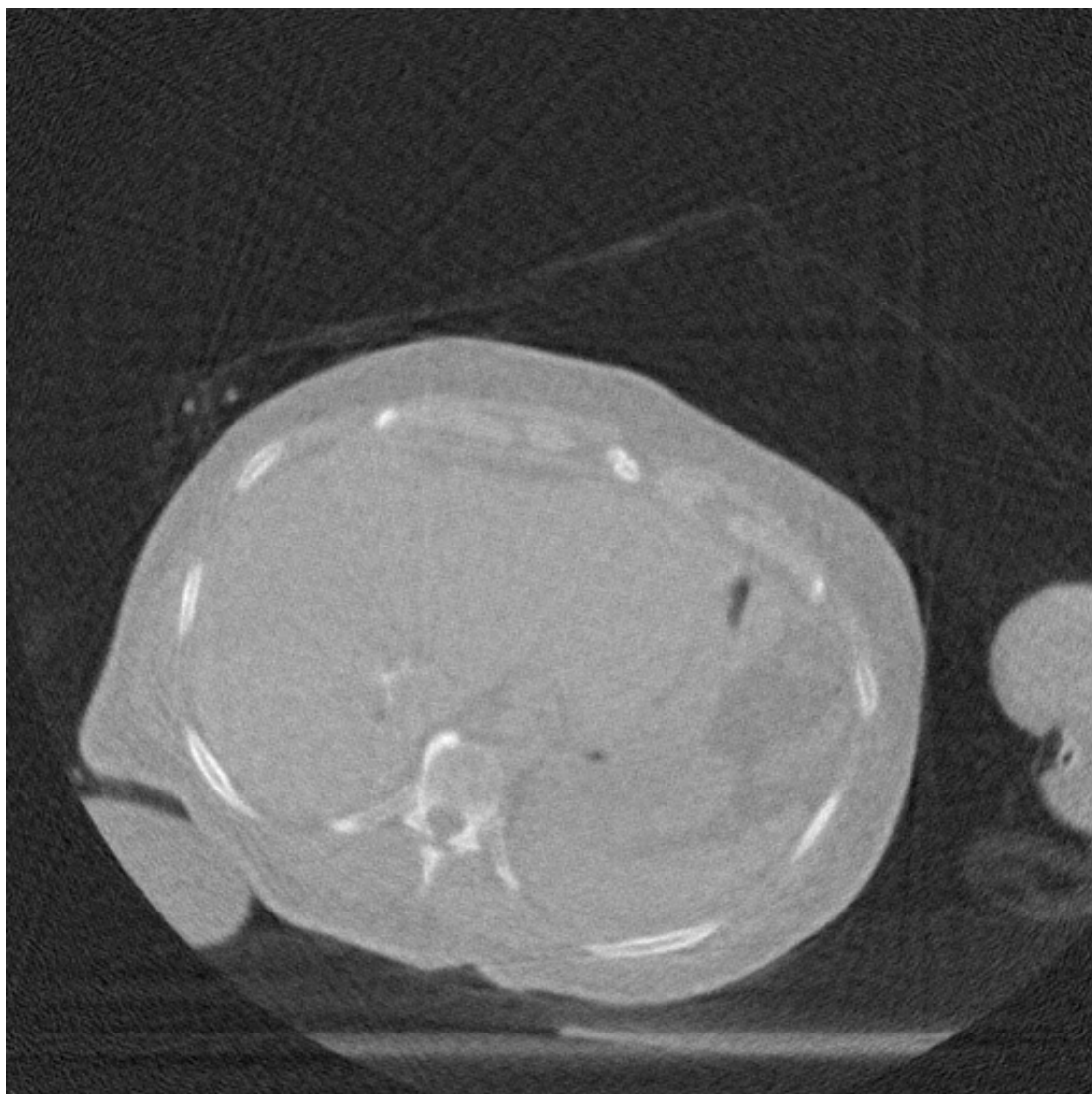
l1-ls

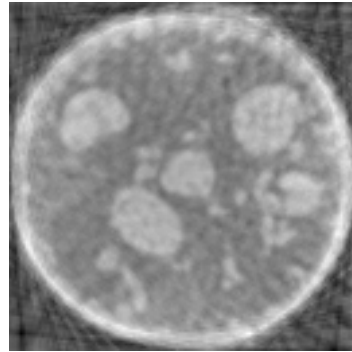Reconstruction result of Figure 2 is shown in large size for better clarity.
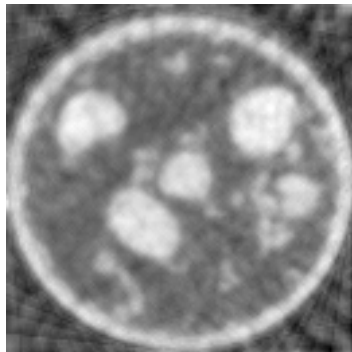

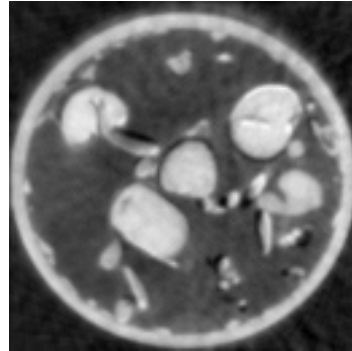Spatially-varying prior method
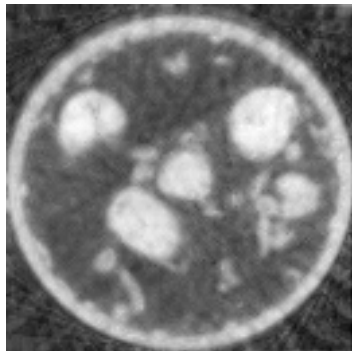
3.2 Sprouts

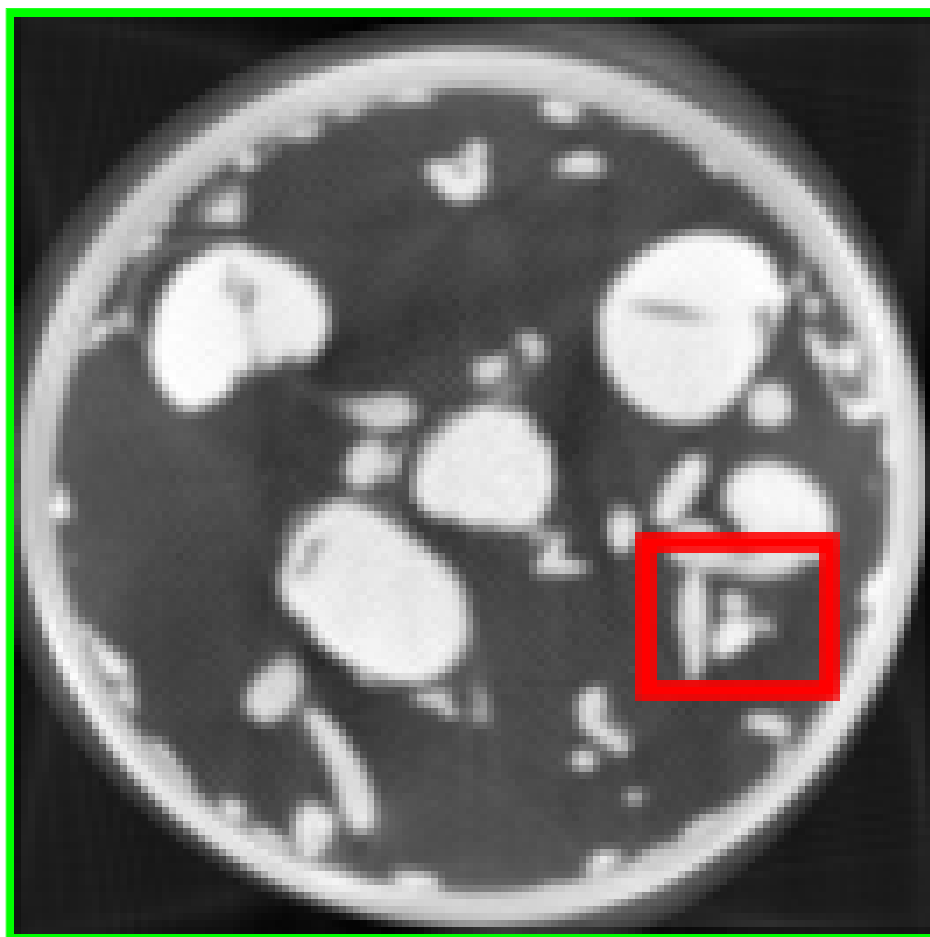(a) Test

(b) FDK

(c) l1-ls

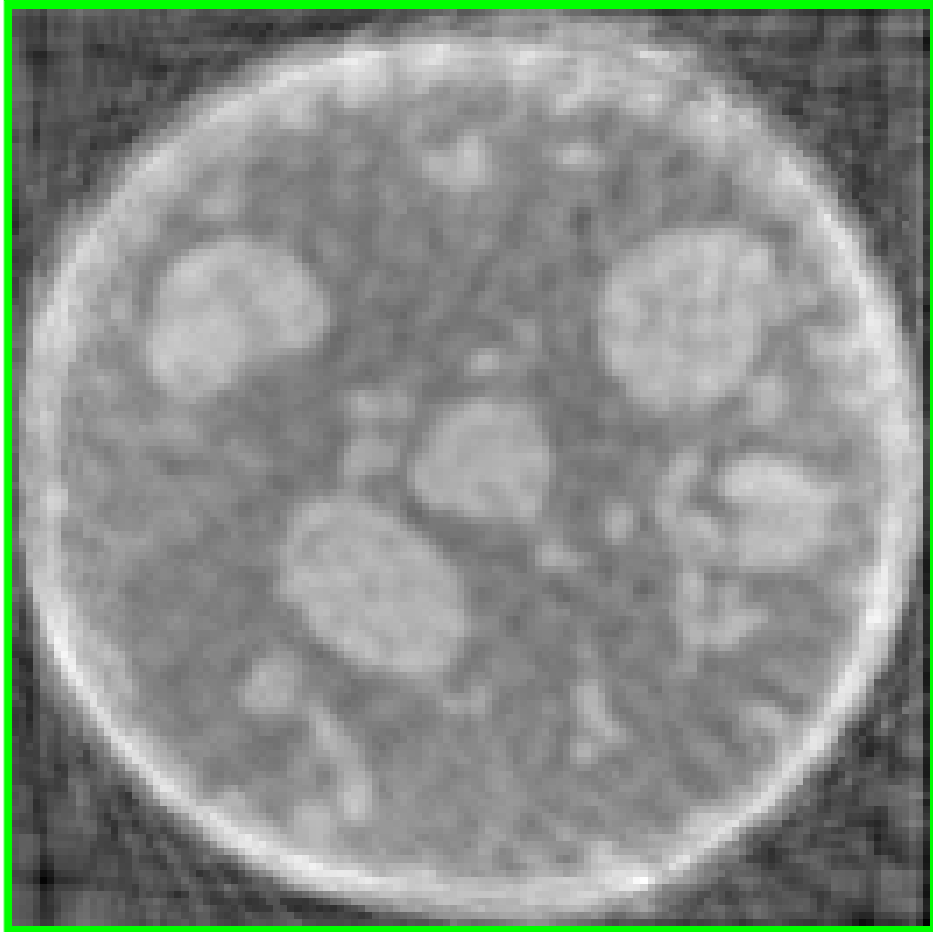(d) Uniform
Prior

(e) Spatially-Varying
prior

Figure 7: Reconstruction of sprouts corresponding to Figure 16 of the main paper.

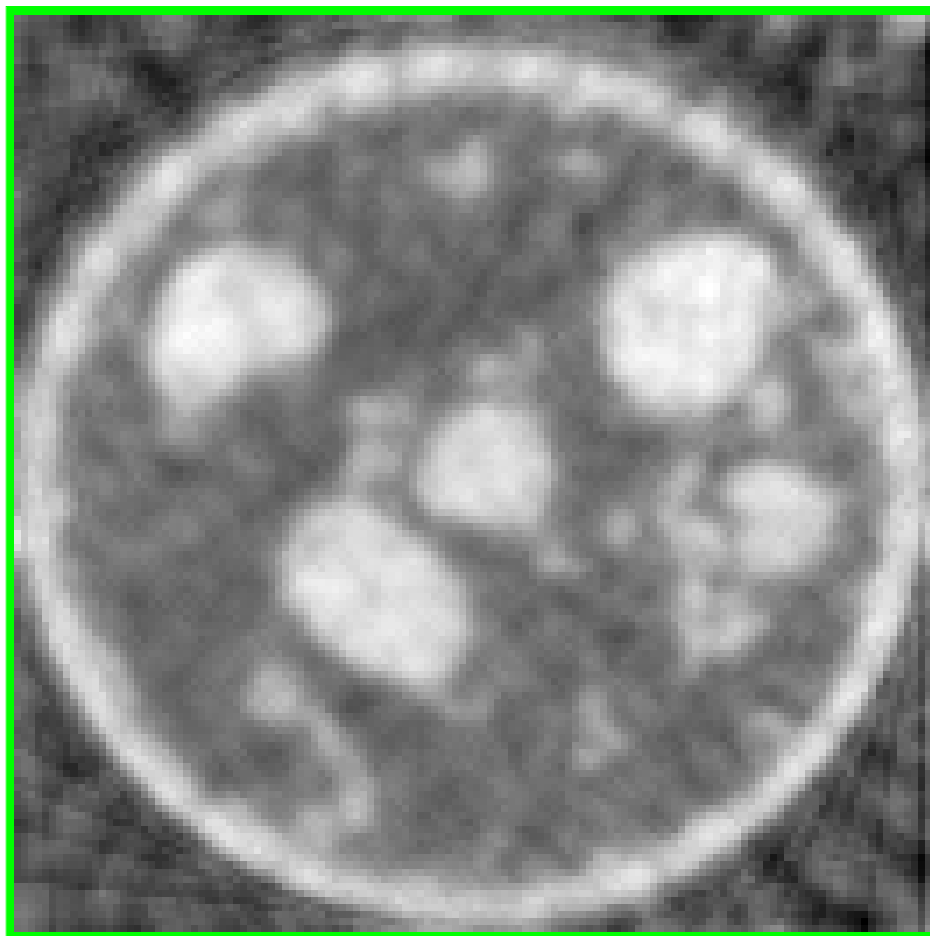**Test image of Figure 7 is shown in large size for better clarity.**

Test

Reconstruction result of Figure **7** is shown in large size for better clarity.

FDK

Reconstruction result of Figure **7** is shown in large size for better clarity.

l1-ls

Reconstruction result of Figure **7** is shown in large size for better clarity.

Uniform Prior

Reconstruction result of Figure **7** is shown in large size for better clarity.

Spatially-Varying Prior

3.3 Okra

(a) Test

(b) FDK, no prior

(c) l1-ls

(d) Uniform prior

(e) Spatially-Varying prior

Figure 13: Reconstruction of okra corresponding to Figure 14 of the main paper.

Test image of Figure 13 is shown in large size for better clarity.

Test

Reconstruction result of Figure 13 is shown in large size for better clarity.

FDK

Reconstruction result of Figure **13** is shown in large size for better clarity.
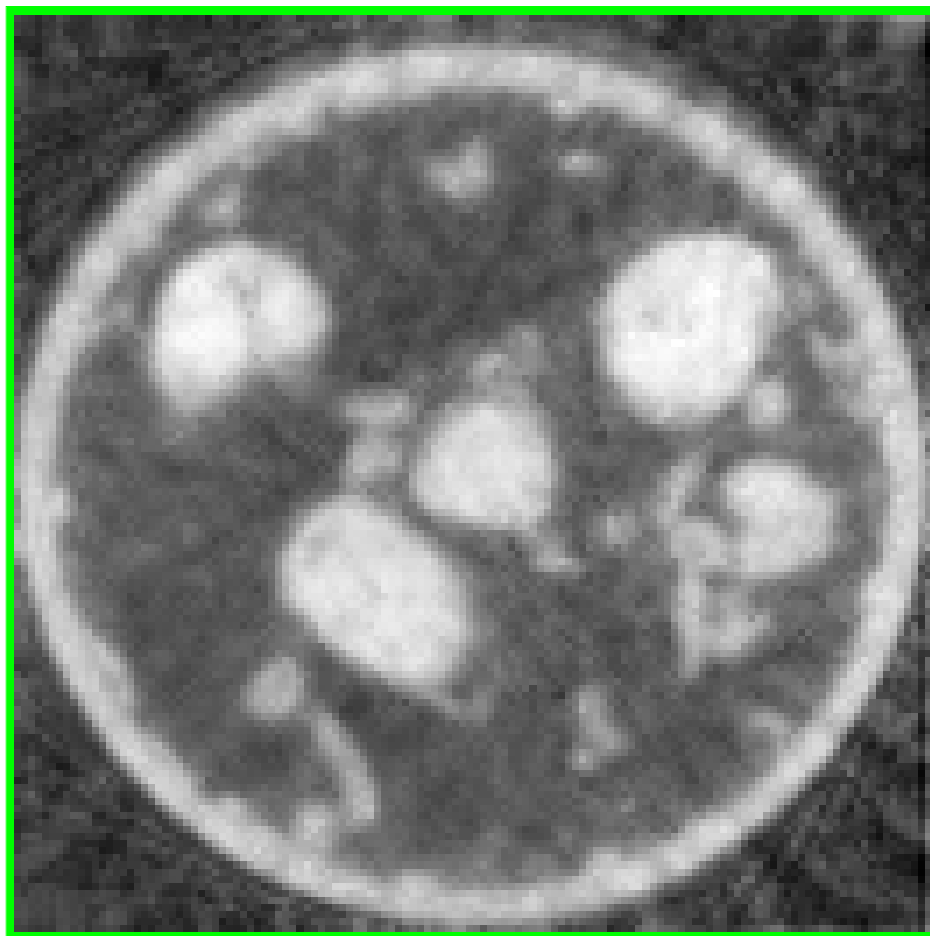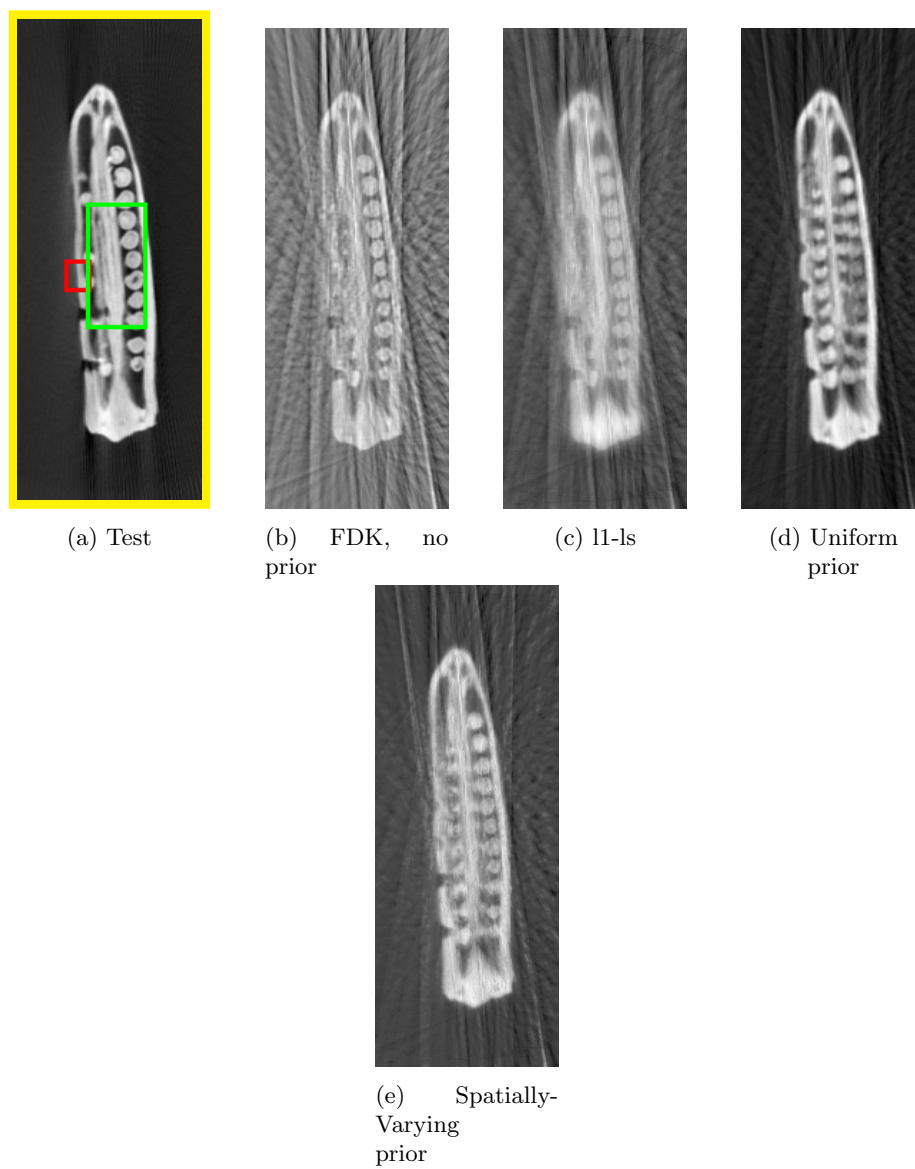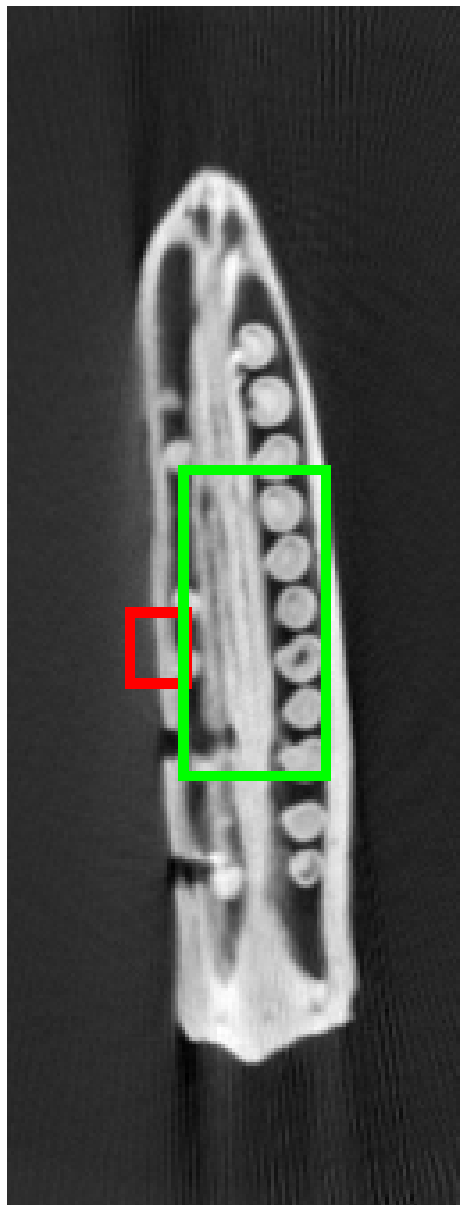

l1-ls

Reconstruction result of Figure 13 is shown in large size for better clarity.

Uniform Prior

Reconstruction result of Figure **13** is shown in large size for better clarity.

Spatially-Varying prior
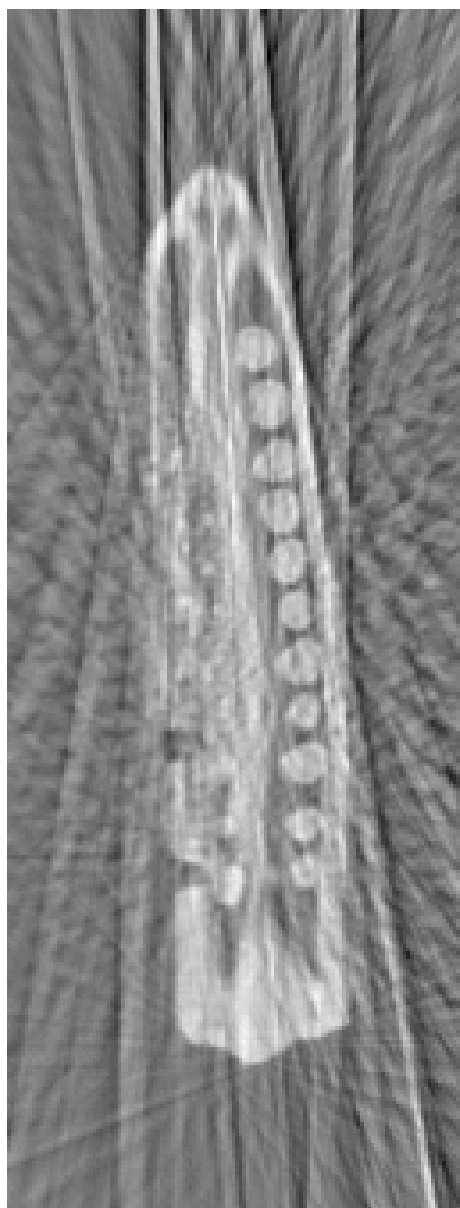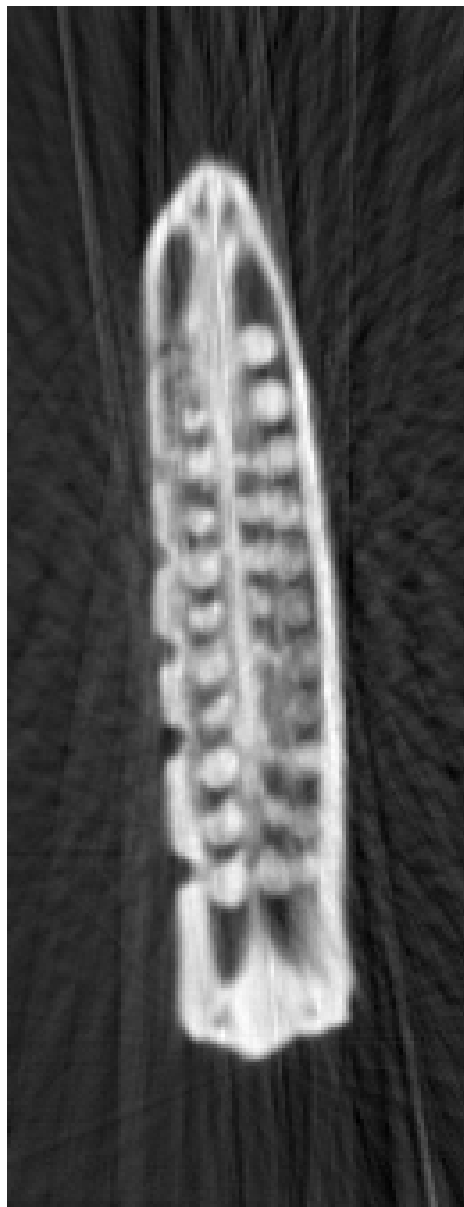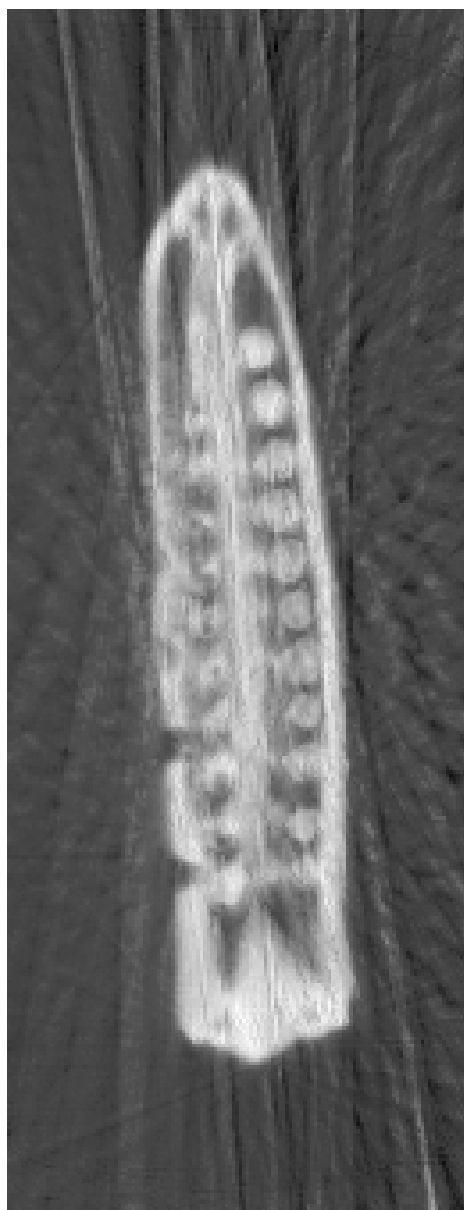
4   Detecting new changes directly in the measurements

Sec.2 of the main paper ('Related work') contrasts the spatially-varying technique with other prior based techniques in literature. Here we present a 2D reconstruction result (of the test shown in Figure. 19) to compare our method with [4], in which the new changes are directly detected in the measurement space by computing the difference between the measurements of the test and the corresponding simulated measurements of the template. This difference-volume is then reconstructed and then fused (added to) with the original high quality template. However, in the above method, the sub-sampling artefacts present in the difference-volume gets carried over to the final reconstructed image. This is shown in Figure 20. A quantitative comparison over the region of interest is shown in Table 1.
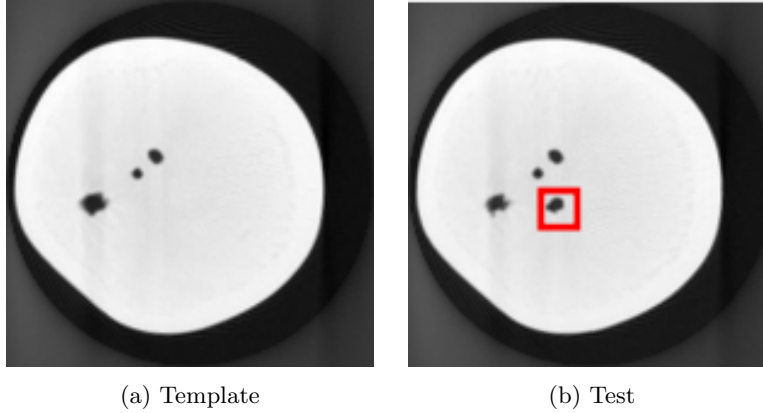

(a) Template   (b) Test

Figure 19: Template and test from the Potato dataset for the reconstructions shown in Figure. 20

(a) [4]:new-changes

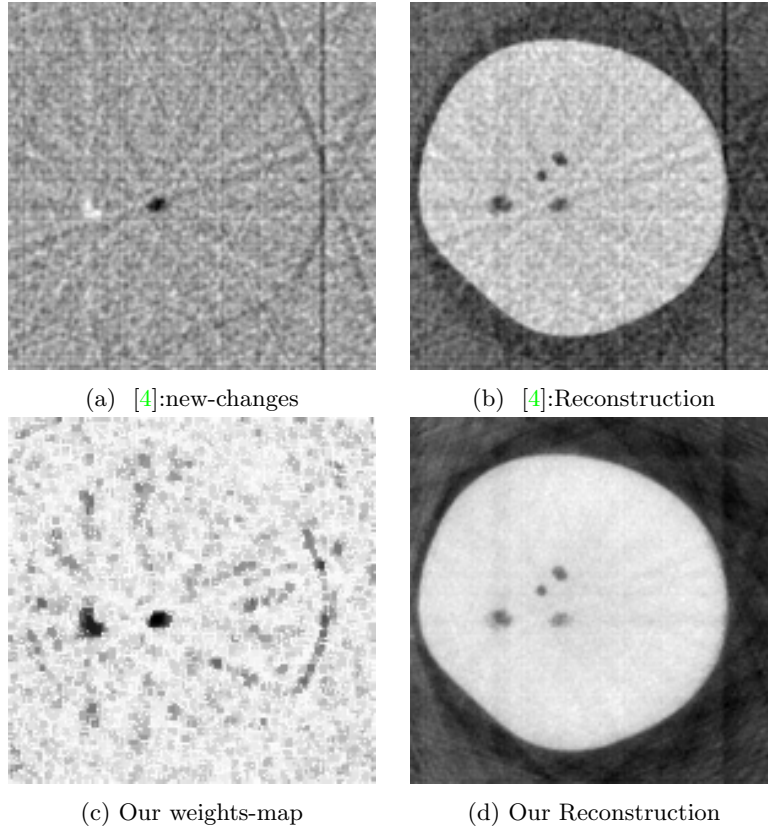(b) [4]:Reconstruction

(c) Our weights-map

(d) Our Reconstruction

Figure 20: Reconstruction of the test in Figure 19. Reconstructions were performed from 12 views. Gaussian noise of 0 mean and SD = 1% of mean of measurements, was added to the measurements.

Table 1: SSIM values (within RoI) of reconstructions shown in Figure 20

	SSIM (whole image)	SSIM (RoI)
Method in [4]	0.65	0.60
Spatially-varying prior	0.89	0.92

5 Blurred reconstruction under limited views

The l1-ls reconstructions shown in the main paper (for example, in Figs. 14(c), 16(c) and 19(c)), appear to be blurred. Here, we discuss the reason for this observation by reconstructing an image from varying number of views using l1-ls (Eq.1 in the main paper).

When the number of views is large, the reconstruction using l1-ls is indeed good, as shown below in Fig 21. For the reconstructions shown below, we have tuned the λ_1 values (Figs. 22, 24, 26) and selected the one with maximum SSIM.

(a) Test   (b) FDK   (c) l1-ls
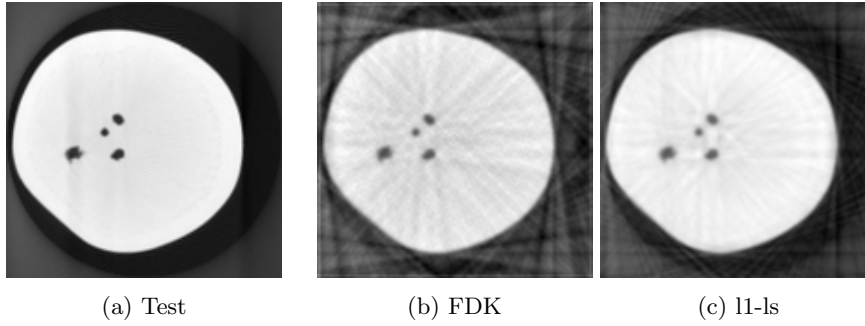
Figure 21: Reconstruction of potato test slice (150×150) from 48 views. The λ_1 for l1-ls reconstruction was chosen to be the optimal value of 0.4 here.
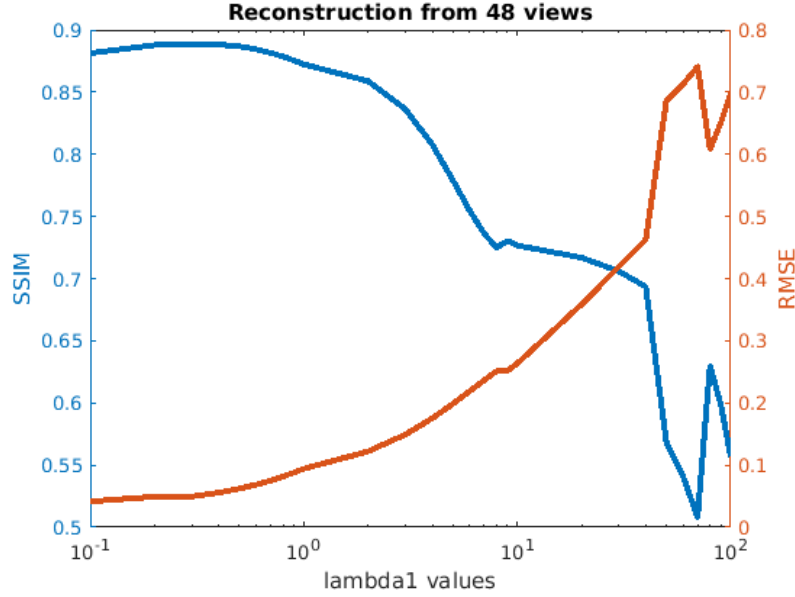
Figure 22: SSIM and RMSE for reconstruction from 48 views for varying levels of λ_1. The optimal value of 0.4 was chosen to obtain the reconstruction shown in Fig. 21

However, when the number of views decreases, the reconstruction using l1-ls is blurred, but with the benefit of suppressed artefacts that are otherwise present in FBP reconstruction. This is illustrated in Figs. 23 and 25.
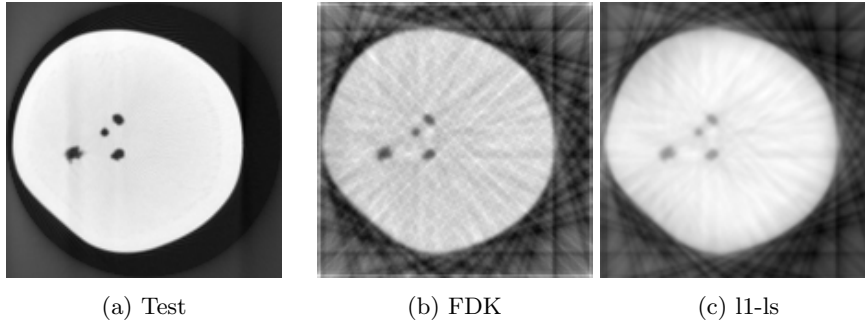

(a) Test   (b) FDK   (c) l1-ls

Figure 23: Reconstruction of potato test slice (150×150) from 24 views. The λ_1 for l1-ls reconstruction was chosen to be the optimal value of 2 here.
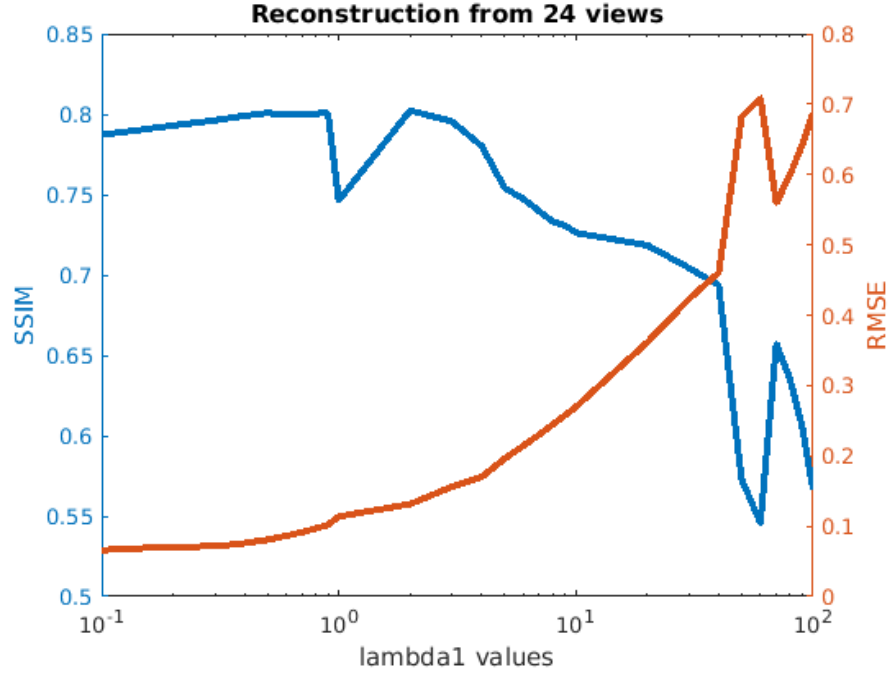
Figure 24: SSIM and RMSE for reconstruction from 24 views for varying levels of λ_1. The optimal value of 2 was chosen to obtain the reconstruction shown in Fig. 23
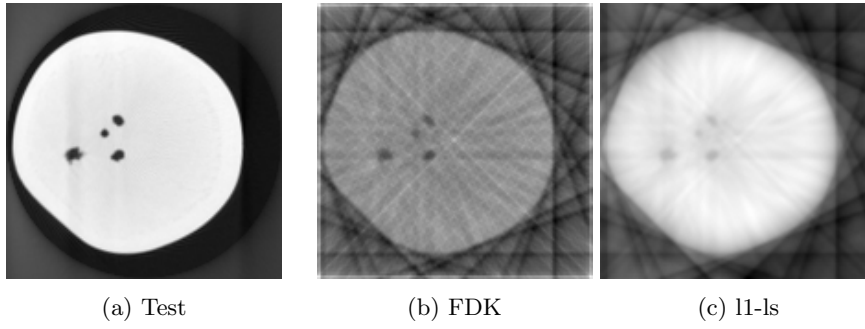

(a) Test   (b) FDK   (c) l1-ls

Figure 25: Reconstruction of potato test slice (150×150) from 12 views. The λ_1 for l1-ls reconstruction was chosen to be the optimal value of 3 here.

As seen here, the reconstruction by l1-ls is indeed blurred when the number of views is very less. The iterative reconstruction was run until convergence (epsilon = 0.001).
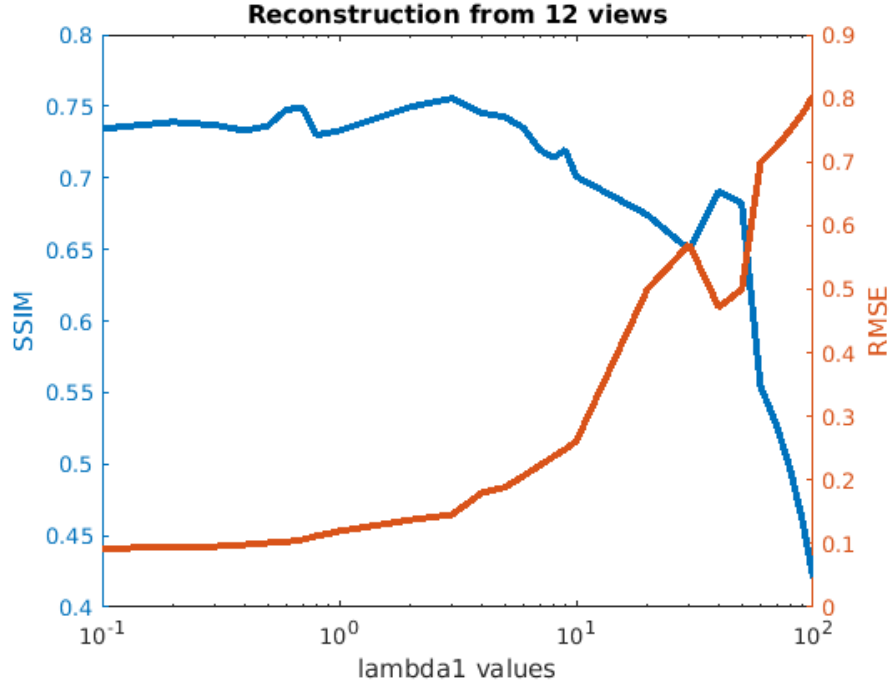
Figure 26: SSIM and RMSE for reconstruction from 12 views for varying levels of λ_1. The optimal value of 3 was chosen to obtain the reconstruction shown in Fig. 25

References

[1] P. Gopal, R. Chaudhry, S. Chandran, I. Svalbe, and A. Rajwade, "Tomographic reconstruction using global statistical priors," in *DICTA*, Sydney, Nov. 2017.

[2] M. Aharon, M. Elad, and A. Bruckstein, "K-svd: An algorithm for designing overcomplete dictionaries for sparse representation," *IEEE Transactions on Signal Processing*, vol. 54, no. 11, pp. 4311–4322, Nov 2006.

[3] K. Koh, S.-J. Kim, and S. Boyd, "l1-ls: Simple matlab solver for l1-regularized least squares problems," https://stanford.edu/~boyd/l1_ls/, last viewed–July, 2016.

[4] J. Lee, J. W. Stayman, Y. Otake, S. Schafer, W. Zbijewski, A. J. Khanna, J. L. Prince, and J. H. Siewerdsen, "Volume-of-change cone-beam CT for image-guided surgery," pp. 4969–89, Aug 2012.